$NO_2\,\tilde{A}\,^2B_2$ state properties from Zeeman quantum beats

P. J. Brucat and R. N. Zare

Department of Chemistry, Stanford University, Stanford, California 94305
(Received 4 August 1982; accepted 22 September 1982)

We have observed the temporal modulation of fluorescence induced by a static magnetic field after selective optical excitation of a single fine structure level via the $\tilde{A}\,^2B_2$–$\tilde{X}\,^2A_1$ electronic transition in NO_2. The rotationally resolved population and alignment decay rates, fluorescence polarization anisotropy, and magnitude and sign of the excited Landé g factor are determined simultaneously from measurement of the Zeeman quantum beats. The importance of the these properties to the description of the $\tilde{A}$ state of NO_2 is discussed.

I. INTRODUCTION

We present the results of a study in which the time evolution of an optically prepared molecule is monitored via its subsequent fluorescence. The spatial anisotropies of this fluorescence are of particular interest when they can be related to intrinsic excited state properties. Time-resolved fluorescence techniques have been used for this purpose on a variety of systems and can sometimes provide a simple demonstration of properties difficult to infer from other methods. One specific type of time-resolved fluorescence technique, that of field-induced fluorescence modulation following pulsed optical excitation (field-induced quantum beats), has been developed over the past 20 years.[1–4] Although many impulsive excitation schemes may be used to generate quantum beats, only optical processes will be considered here.

The phenomenon of field-induced quantum beats is well understood. Magnetic field-induced beats, called Zeeman quantum beats, were first directly observed in the fluorescence from $^3P_1$ levels of Cd[5] and Hg.[6] These experiments demonstrated the existence of the effect but were plagued by poor sensitivity due to the low intensity and inadequate temporal quality of the shuttered resonance lamp sources used for excitation. Pulsed dye laser excitation was shown to be far more desirable by Gornik *et al.*[7] who demonstrated that Zeeman quantum beats could be observed in the fluorescence from Yb $6\,^3P_1$ with good signal-to-noise after a single laser shot. The analogous electric-field-induced quantum beam phenomenon (Stark quantum beats) was first demonstrated by Hese *et al.*[8] in fluorescence from Ba $6\,^1P_1$.

These early experiments on atomic systems proved not only that field-induced quantum beats were experimentally observable but that they were fully in agreement with quantum mechanical predictions of the interaction of the atom with the applied field and the spatial properties of electric dipole absorption and emission. Emphasis was placed on the comparison of the excited state energy splitting in the field measured by quantum beat techniques with that measured by other techniques. In all cases the quantum beat results were in accord with the best available data.

Quantum beats from molecules are more difficult to observe than from atoms due to the weaker transition probability for a single rotational line, the reduced amplitude of fluorescence modulation, and the more complicated beat pattern. Nonetheless, Wallenstein *et al.*[9] observed Zeeman quantum beats from several (v', J') levels of the $I_2\ B\,^3\Pi(0_u^+)$ and used the technique to determine the variation of the Landé g factor with vibrational excitation. The vibrational dependence of the electric dipole moment of the $A\,^1\Sigma^+$ state of LiH was determined by Brieger *et al.*[10] in the first published account of Stark quantum beats in molecular fluorescence. Other molecules studied by field-induced quantum beats include Se_2,[11] OH,[12] NaH,[13] and BaO.[14]

The $\tilde{A}\,^2B_2$ state of NO_2 is an infamous example of a state that has been extensively studied by numerous spectroscopic methods[15] but still eludes understanding. The vibrational-rotational structure of this state is complex and highly perturbed. The $\tilde{A}$ state is one of four low-lying electronic states that are thought to be mixed both vibronically and by Renner–Teller interaction.[16] Even the radiative lifetime of the $\tilde{A}$ state has been a matter of controversy following the observation that an apparent discrepancy exists between the directly observed radiative decay rate and the rate derived from the integrated absorption strength of the $\tilde{A}$–$\tilde{X}$ system.[17] Perhaps the most disturbing result regarding the radiative properties of NO_2 was the observation of nonexponential fluorescence decay from a single hyperfine level excited under collisionless molecular beam conditions.[18] Although not statistically predicted for this size molecule,[19] irreversible radiationless processes are one possible explanation for this behavior.

Various coherence experiments on the $\tilde{A}$ state of NO_2 have yielded startling and theoretically unexpected results. Zero-field level crossing experiments[20] in conjunction with optical radio frequency double resonance[21] indicate that the decay of spatial coherence of the excited state may be more rapid than radiative decay under conditions approaching isolation. However, recent experiments have contradicted this.[22] In addition, magnetic field decoupling experiments suggest the existence of a number of closely spaced levels all having the same total angular momentum, called a "bunch" structure.[23] Moreover, the observed Landé g factors appear to follow theory based on simple angular momentum coupling arguments for some rotational levels and not for others.[21,22]

 0021-9606/83/010100-12$02.10

In this study we show that the measurement and interpretation of magnetic field-induced quantum beats from the NO_2 $\tilde{A}$ state provide a direct resolution of some of the outstanding controversies concerning the radiative, magnetic, and coherence properties of this molecular state.

II. DESCRIPTION OF THE EFFECT

The physical basis for the modulation of fluorescence in the presence of an applied magnetic field under the conditions of this experiment can be explained in a simple picture of isolated, electronically excited molecules possessing a permanent magnetic moment μ lying along the total angular momentum $\mathbf{J}'$. Linearly polarized laser excitation can produce an ensemble of these excited molecules with one specific $\mathbf{J}'$ that is *aligned* with respect to the laser electric field (see Fig. 1). It has been shown that the fluorescence from such an ensemble is spatially anisotropic[24] and the magnitude of this anisotropy depends on the change in total angular momentum upon absorption and emission.[25]

The application of a homogeneous magnetic field H to the ensemble would classically result in Larmor precession about the field axis $\hat{z}$. That is to say, the angular momentum $\mathbf{J}'$ of each excited molecule in the ensemble is now stationary in a rotating frame with angular frequency ω_L, where

$$\omega_L = \gamma H = g\mu_0 H/\hbar \ . \tag{1}$$

The emission intensity pattern from the ensemble is then also stationary in this frame.

Assume now that conditions are chosen such that the radiative lifetime of the emitters is much longer than the precession period, which in turn is longer than the duration of the excitation ($\tau_R \gg \omega_L^{-1} \gg T$). The precessional motion of the emission pattern would then produce a temporal modulation at $2\omega_L$ in the intensity observed by a lab-fixed detector with the geometry shown in Fig. 1. The modulation frequency at the detector must be at *twice* the Larmor frequency because the anisotropy produced in the ensemble after linearly polarized excitation transforms under rotation as a quadrupole moment, repeating itself every π radians. The detected modulation will be maximized when the components of the excitation and detection polarization along the field axis are minimized, i.e., when the excitation and emission polarizations are chosen perpendicular to the field direction.

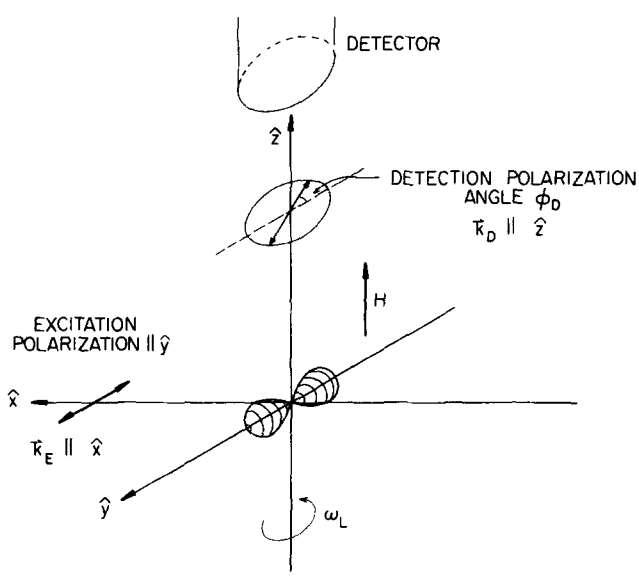

FIG. 1. Excitation/detection geometry for the observation of Zeeman quantum beats. The polarized light pulse produces an anisotropic ensemble of excited states (shown schematically at time $t=0$ as a dumbell) which precesses in space at ω_L due to the magnetic field H. Fluorescence passing the detection polarizer has a temporal modulation proportional to $\cos[2(\omega_L t + \phi_D)]$.

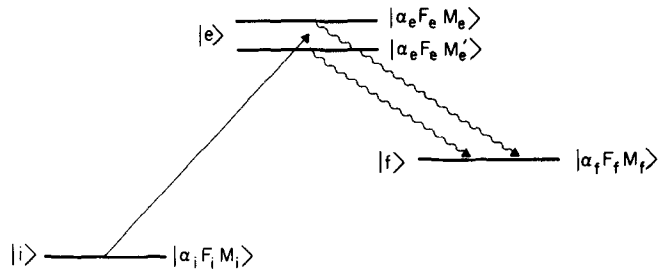

FIG. 2. Level scheme exemplifying the interference observed in a Zeeman quantum beat experiment. Fluorescence from the coherently excited magnetic sublevels of the state $|e\rangle$ exhibits modulation at their frequency difference.

Although the classical treatment of the evolution of the excited molecule gives us a good qualitative understanding of the field-induced quantum beat signal, we recognize that for quantitative understanding of the phenomenon we must use a quantum description that takes into account the quantization of the total angular momentum of the system in magnitude (J) and space (M). The general phenomenon of "quantum beats" gets its name from the quantum mechanical concept of interference between a coherently excited superposition of states manifesting itself in the temporal modulation or "beating" of some observable at the difference frequencies of the states composing the superposition. Figure 2 shows a level scheme that describes the type of interference observed in this study. The initial state of the system $|i\rangle$ is labeled by its total angular momentum F_i, and F_i's projection on a space fixed axis M_i (α_i denote all other quantum numbers). A short optical excitation pulse connects the excited state $|e\rangle$ with the initial state $|i\rangle$ via the electric dipole operator. If the excitation pulse is sufficiently short and has the proper polarization, the excited state $|e\rangle$ will be a superposition of states $|\alpha_e F_e M_e\rangle$ and $|\alpha_e F_e M_e'\rangle$. These excited states are nondegenerate due to the presence of an applied magnetic field (chosen along the quantization axis). The evolution of the excited state will include spontaneous emission to the final state $|f\rangle$. If the fluorescence from $|e\rangle$ to $|f\rangle$ is observed with the proper polarization, the intensity will be modulated at the difference frequency between the levels $|\alpha_e F_e M_e\rangle$ and $|\alpha_e F_e M_e'\rangle$. If either the excitation or the detection polarization is parallel to the applied field (quantization axis), no quan-

tum beats are exhibited because the $\Delta M = 0$ selection rule in absorption and emission for those polarizations cannot allow interference. For excitation and detection polarizations perpendicular to the field, the $\Delta M = \pm 1$ selection rule implies that modulation will be observed at the frequency separation of the levels $|e\rangle$ with M_e differing by two.

Even if a single F_i, F_e pair can be selected in excitation, the fluorescence observed in the real experiment will consist of the sum over all possible M_i, M_e, F_f, and M_f quantum numbers. The evaluation of this sum rapidly becomes tedious even for moderate values of F_e. Some review articles concerning the subject of optically produced coherence include Alexandrov,[1] Haroche,[2] Lehmann,[3] and Dodd and Series.[4]

A superior way to describe the mechanics of an ensemble of molecules exhibiting coherence is through the density operator formalism.[26] To take maximum advantage of the rotational symmetry of the problem we introduce state multipoles by using a spherical irreducible tensor basis for this density matrix:

$$T^{F'F}_{kq} = \sum_{M',M} (-1)^{F'-M'} (2k+1)^{1/2} \begin{pmatrix} F' & F & k \\ M' & -M & -q \end{pmatrix} \times |\alpha F' M'\rangle\langle \alpha F M| \ . \tag{2}$$

In what follows we outline the derivation of explicit formulas which describe the preparation, evolution, and detection of the excited state multipoles. These formulas are central to the analysis of the Zeeman quantum beat signals we observe.

Consider the subblocks of the density matrix ρ,

$$\rho_n = \langle n|\rho|n\rangle |n\rangle\langle n|; \ n = i, e, f \ . \tag{3}$$

Before the arrival of the laser pulse the system is in thermal equilibrium with its surroundings, which means ρ_e, ρ_f are zero as are all off-diagonal elements of ρ. Only the diagonal $k = q = 0$ terms in ρ_i are nonzero. If the excitation duration T is sufficiently short we may ignore the evolution of the system caused by the presence of the magnetic field and spontaneous emission or collisions leading to relaxation during the time ρ_i and ρ_e are coupled via the optical field. Consider the excitation process, for now, in terms of the subblocks of ρ without regard to their "internal" structure. The factored equation of motion for ρ then appears during the laser pulse as an undamped two-level system:

$$\dot{\rho} = \frac{1}{i\hbar} [\mathcal{H}, \rho] \ ,$$

$$\mathcal{H} = \begin{bmatrix} \mathbf{E}_f & 0 & 0 \\ 0 & \mathbf{E}_e & \mathbf{D} \\ 0 & \mathbf{D}^* & \mathbf{E}_i \end{bmatrix} \ , \tag{4}$$

$$\mathbf{D} = -\tfrac{1}{2} \langle e|\hat{\epsilon}_1 \cdot \mathbf{r}|i\rangle e\mathcal{E}_0 \exp[-i(2\pi\nu_0)t] \ .$$

The $\mathbf{E}_n$ are the diagonal eigenvalue matrices for the subblocks ρ_n and $\mathbf{D}$ is the matrix of the electric dipole operator in the rotating wave approximation. For the condition of broadband excitation, we recognize

$$\pi\Delta\nu_0 \gg 1/T \gg \omega_{e,e'} \ . \tag{5}$$

Here, the pulse averaged spectral bandwidth is $\Delta\nu_0$, and the maximum frequency span of interest in the internal structure of ρ_e is $\omega_{e,e'}$. In analogy to the solution for the two-level system[27] the flow of population from ρ_i to ρ_e under the condition of slowly varying populations follows a rate equation

$$\frac{\partial}{\partial t} \mathrm{Tr}[\rho_e] = -\frac{\partial}{\partial t} \mathrm{Tr}[\rho_i] = R \, \mathrm{Tr}[\rho_i - \rho_e] \ . \tag{6}$$

Linear response of the system to the light field is assured if the integrated rate over the laser pulse remains small, i.e.,

$$RT = \left\{ \frac{1}{2} \frac{\mathrm{Tr}[|\mathbf{D}|^2]}{\hbar^2(\pi\Delta\nu_0)} \right\} T \ll 1 \ . \tag{7}$$

For a laser pulse that lasts from $-T$ to 0 the excited state produced by the excitation is then

$$\rho_e(t=0) = A\langle e|\hat{\epsilon}_1 \cdot \mathbf{r}|i\rangle\langle i|\hat{\epsilon}_1^* \cdot \mathbf{r}|e\rangle \, |e\rangle\langle e| \ . \tag{8}$$

Here, A is a constant determining the strength of the excitation. Therefore we see that all of the behavior of the excited state produced in the excitation is embodied in the operator

$$\Lambda = |e\rangle\langle e|\hat{\epsilon}_1 \cdot \mathbf{r}|i\rangle\langle i|\hat{\epsilon}_1^* \cdot \mathbf{r}|e\rangle\langle e| \ , \tag{9}$$

to which $\rho_e(t=0)$ is proportional.

The angular dependence of the operator Λ has been worked out in general.[28] We wish to consider the case for which the state ρ_i is isotropic and for which we do not excite coherence between levels of different total angular momentum F (i.e., ρ_e spans only one $F_e \equiv F$). Here, the excited state produced by linearly polarized light parallel to the quantization ($\hat{z}$) axis contains only two terms

$$\rho_e(t=0) = \langle T^{FF}_{00}\rangle + \langle T^{FF}_{20}\rangle \ . \tag{10}$$

If we instead excite with linearly polarized light perpendicular to $\hat{z}$ the excited state must be described by four terms

$$\rho_e(t=0) = \langle T^{FF}_{00}\rangle + \langle T^{FF}_{20}\rangle + \langle T^{FF}_{22}\rangle + \langle T^{FF}_{2-2}\rangle \ . \tag{11}$$

The time evolution of the excited state in a magnetic field applied along the $\hat{z}$ axis ($t > 0$) under the first order Zeeman Hamiltonian

$$\mathcal{H}_{\mathrm{Zeeman}} = g_F \mu_0 M_e H = \hbar \omega_L M_e \tag{12}$$

can be shown[29] to take the form

$$\langle T^{FF}_{kq}(t)\rangle = \exp(-iq\omega_L t)\langle T^{FF}_{kq}(t=0)\rangle \ . \tag{13}$$

Thus we see that the excited state described by Eq. (10) does not exhibit field-induced time dependence whereas that described by Eq. (11) does, consistent with the geometrical argument presented earlier.

We introduce the relaxation of ρ_e due to spontaneous emission phenomenologically as an exponential decay with an empirical decay rate. In the absence of other processes all state multipoles (irreducible tensor components) of ρ_e will decay with the same rate constant. If collisions occur whose center of mass ve-

locity in the lab frame is random, each state multipole will decay in general with a rate dependent on k but not q.[30] Therefore, from Eq. (11),

$$\rho_e(t) = \langle T_{00}^{FF}\rangle \exp(-\Gamma_0 t) + [\langle T_{00}^{FF}\rangle + \langle T_{22}^{FF}\rangle \exp(-i2\omega_L t) + \langle T_{2-2}^{FF}\rangle \exp(+i2\omega_L t)]\, e^{-\Gamma 2t} \ . \tag{14}$$

The probability of detection of a fluorescence photon at time t will be the expectation value of the detection operator Δ.

$$\langle\Delta\rangle = T_r(\rho\Delta) \ ,$$
$$\Delta = B\,|e\rangle\langle e|\hat{\epsilon}_2\cdot\mathbf{r}\,|f\rangle\langle f|\hat{\epsilon}_2^*\cdot\mathbf{r}\,|e\rangle\langle e| \ , \tag{15}$$

where B is a constant proportional to the detection efficiency. Note that the form of Δ is identical to that of Λ [Eq. (9)] and the general solution for its matrix elements[28] may be applied again. Since the final state is not selected in this experiment (i.e., the final state is not detected in coincidence with the fluorescence), only the $k = q = 0$ term in ρ_f contributes to the matrix elements of Δ. Therefore, the field-induced temporal modulation of the fluorescence signal depends on the Zeeman effect in the excited state ρ_e *only*.

Using the explicit forms[28] of the operators Λ and Δ one can obtain the fluorescence intensity at the detector for the case of excitation and detection polarizations perpendicular to the magnetic field[31]:

$$I(t) = C\left[\begin{Bmatrix} 0 & 1 & 1 \\ F_i & F_e & F_e \end{Bmatrix}\begin{Bmatrix} 0 & 1 & 1 \\ F_f & F_e & F_e \end{Bmatrix} e^{-\Gamma_0 t} + \frac{1}{2}\begin{Bmatrix} 2 & 1 & 1 \\ F_i & F_e & F_e \end{Bmatrix}\begin{Bmatrix} 2 & 1 & 1 \\ F_f & F_e & F_e \end{Bmatrix} \times[1 + 3\cos[2(\omega_L t + \phi_D)]]\, e^{-\Gamma 2t}\right]. \tag{16}$$

Here, C is a constant proportional to the strength of the excitation, the detection efficiency, and the rotational line strengths of the transitions, and ϕ_D is the angle between the excitation $\hat{\epsilon}_1$ and detection $\hat{\epsilon}_2$ polarizations (see Fig. 1). The Doppler limited excitation conditions of this study require that Eq. (16) be summed over the $(2I + 1 = 3)$ F_e values corresponding to a single fine structure state and all relevant F_i, F_f values weighted by the appropriate line strength relations.

To complete this analysis, we need to relate the Larmor frequency ω_L to the internal structure of the state $|\alpha_e F_e\rangle$. If the energy separations between the hyperfine levels are large compared to the natural linewidth and yet small compared to the spin-rotation splitting, then the g_F factors of these levels have the relation[32]

$$g_F = g_J \frac{F(F+1) + J(J+1) - I(I+1)}{2F(F+1)} \ . \tag{17}$$

Here, g_J is the g factor of the state labeled by the total angular momentum J if nuclear spin were not present. Furthermore, if Hund's case b coupling is assumed for the $\tilde{A}$ state of NO_2 ($\mathbf{J} = \mathbf{N} + \mathbf{S}$) similar arguments for the coupling of nuclear rotation **N** to electronic spin **S** lead to the relation between g_J and the g factor of the free electron g_e:

$$g_J = g_e \frac{J(J+1) + S(S+1) - N(N+1)}{2J(J+1)} = \pm\frac{(2.0023)}{2N+1} \ ; \quad J = N \pm \tfrac{1}{2} \ . \tag{18}$$

Implicit in the derivation of Eqs. (17) and (18) is the assumption that the magnetic moments associated with the angular momenta **N** and **I** are negligibly small compared to the magnetic moment of the total electron spin **S**.

Thus, under certain assumptions, the magnetic field-induced fluorescence modulation observed in this study can be completely understood with respect to its geometrical properties, amplitude and phase of the modulation [Eq. (16)] and frequency of modulation [Eqs. (1), (17), and (18)].

III. EXPERIMENTAL

A sample of NO_2 at 300 K and at total pressures ranging from 2×10^{-5} to 5×10^{-3} Torr is excited by a single-mode Ar^+ laser pumped R6G dye laser with free running bandwidth of 50 MHz. Laser pulses are produced by an extra-cavity acousto-optic modulator with 20 ns rise and fall times and on/off extinction ratio of greater than 2×10^3. Laser pulses have typical peak powers of 30 mW, 150 ns to 1.0 μs duration, and a repetition period of 200 to 600 μs. The laser beam (0.2 cm in diameter) enters a multipass fluorescence cell in the $-x$ direction immediately following passage through a Glan–Thompson polarizer oriented to pass the electric field in the y direction (see Fig. 1). The laser light is reflected approximately 20 times (optical path $\approx$400 cm) and exits counterpropagating to the incoming beam with polarization $I_y/I_x > 10^2$ and beam diameter about 0.5 cm.

Laser frequencies and NO_2 line positions in the region of 16 850 cm^{-1} were determined from simultaneous Doppler limited excitation spectra of NO_2 and I_2, using the I_2 spectral atlas of Gerstenkorn and Luc.[33]

The sample cell itself consists of a stainless steel, aluminum, brass and Delrin vessel pumped by a liquid nitrogen trapped 2 in. diffusion pump with a base pressure of $\approx 1\times10^{-6}$ Torr. NO_2 pressures of between 2×10^{-5} and 1×10^{-4} Torr were maintained in a conduction-limited slow flow. Foreign gases can be added via an auxiliary inlet. Chamber pressure was monitored by an ionization gauge and capacitance manometer (Baratron 220B 1 Torr absolute head, PDR-C-1B controller).

The chamber is surrounded by two sets of 1 m Helmholtz coils (x, y directions) and on set of 35 cm Helmholtz coils (vertical = z direction). Magnetic fields in the chamber are measured with a HP Model 428B Clipon microammeter with 3529 A magnetometer probe. Absolute calibration of this magnetometer is made by measurement of the field produced by a standard solenoid coil (7.7 cm diameter, 33.5 cm long, 11.32 windings per cm) at a known current (determined by a Keith-

ley Model 179 TRMS digital multimeter). Applied chamber magnetic fields are determined during the course of the experiment via an empirical coil current vs field calibration formula. Field inhomogeneity is ±3 mG over the detection volume and accurate to ±1%.

Fluorescence was detected by a cooled (−20 °C) S-20 response photomultiplier tube (Centronix Q4283 SA-25) via glass window, HN-32 sheet polarizer, lens, and Corning 2-58 red cutoff filter, in that order, along the $+z$ direction. Choice of polarizer angle ϕ_D determined the initial phase of the fluorescence modulation with respect to the laser pulse. The detection system is sensitive to emission from about 620 to 850 nm in a volume with mean diameter of approximately 8 cm centered in the chamber.

The emission was time resolved using a time to pulse height converter/multichannel analyzer (Ortec 467/Nicolet 1070) or fast multichannel scalar (Nicolet 1170) pulse counting electronics. The time response of the phototube TPHC/MCA system is calibrated on the 160 μs time scale by double pulsing the laser and observing laser scatter in the cell. The measured time between laser pulses on this system is compared with that measured by a fast photodiode and an HP 5315A universal counter. The former is 0.5% less than that of the latter; this is considered insignificant and is subsequently ignored. Fluorescence decays are recorded with 1024 channel resolution with full scale ranges from 160 μs to 1 ms.

Decay data arrays are transferred to an Apple II microcomputer for manipulation. Data handling consists of:

(1) Deconvolution of pulse pile-up error in the TPHC/MCA system; (2) Baseline correction for dark counts and modulator leakage; (3) Subtraction of laser scatter from the fluorescence decay; (4) Linear least squares fit of ln (Intensity) vs time to obtain fluorescence decay rates; (5) 1024 point complex fast Fourier transform of the decay; (6) Deconvolution of the transformed data for finite excitation pulse duration.

Not all these procedures were performed on any particular data set.

IV. RESULTS

Figure 3 shows a laser fluorescence excitation (LFE) spectrum of NO_2 at room temperature in the region of the origin of a prominent although vibrationally unassigned band usually denoted as the 5933 Å band. It should be noted that the fluorescence excitation spectrum of NO_2 may differ markedly from its absorption spectrum due to the reduced detection efficiency for very long lived and/or very red shifted fluorescing states. However, the LFE spectrum would be expected to adequately represent the relative absorption probabilities of transitions within a particular vibronic band. The Doppler width of NO_2 at 300 K is 920 MHz and the resolution element of this spectrum is 400 MHz (the laser cavity FSR) so this spectrum is essentially Doppler limited. There is no laser frequency between 16 825 and 16 880 cm^{-1} that fails to produce fluorescence on the order of 5% of that of the strong transitions in the 5933 Å band. Note that this implies an absorption transition density of at least 30 transitions/cm^{-1}. Thus, it is clear that even 50 MHz excitation bandwidth does not imply selective excitation of a single fine structure level due to overlapping absorptions.

The rotational assignments of many transitions in the 5933 Å band have been made[34,35] and these assignments form a starting point for this study. The band is an a-type (ΔK_a = even; ΔK_c = odd) vibronic transition between two nearly prolate asymmetric rotor states. Indicated in Fig. 3 are the P and R transitions connecting the (vibrationless[36]) $\tilde{X}\,^2A_1$ ground state to the two fine structure components of the $3_{03}(N' = 3,\ K_a' = 0,\ K_c' = 3)$ rotational level in the $\tilde{A}\,^2B_2$ state. These P and R branch members straddle the unresolved Q branch (allowed for $K_a' > 0$) near 16 849 cm^{-1}. The $K_a' = 0$ stack for N' = odd (N' = even are missing due to nuclear spin statistics) can be seen in the P branch as a prominent series of doublets with spin splitting increasing with N' marching out to the red of the band origin. This

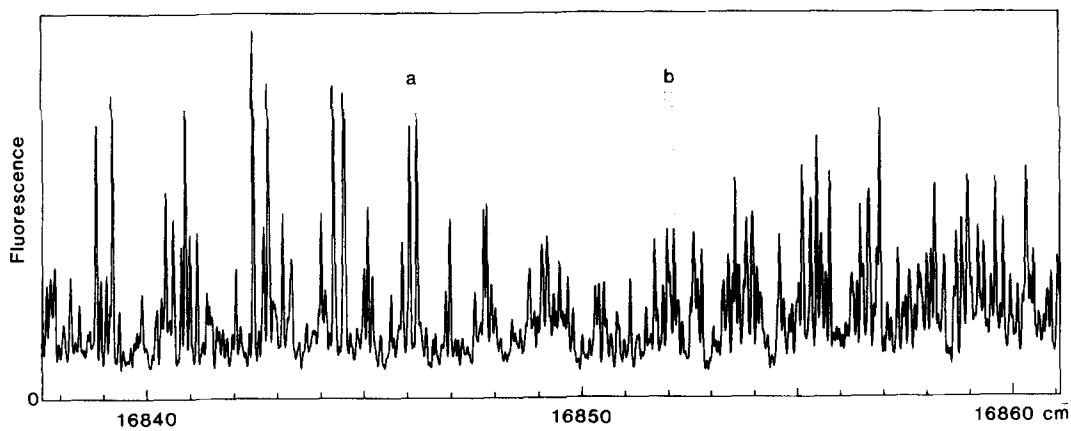

FIG. 3. Laser fluorescence excitation spectrum of NO_2 at room temperature and low pressure ($< 1\times10^{-4}$ Torr). The features marked "a" and "b" are spin doublets of the $3_{03}-4_{04}$ and $3_{03}-2_{02}$ transitions, respectively. In each doublet the low frequency component is F_1 ($J = N + \frac{1}{2}$) and the other is F_2 ($J = N - \frac{1}{2}$).

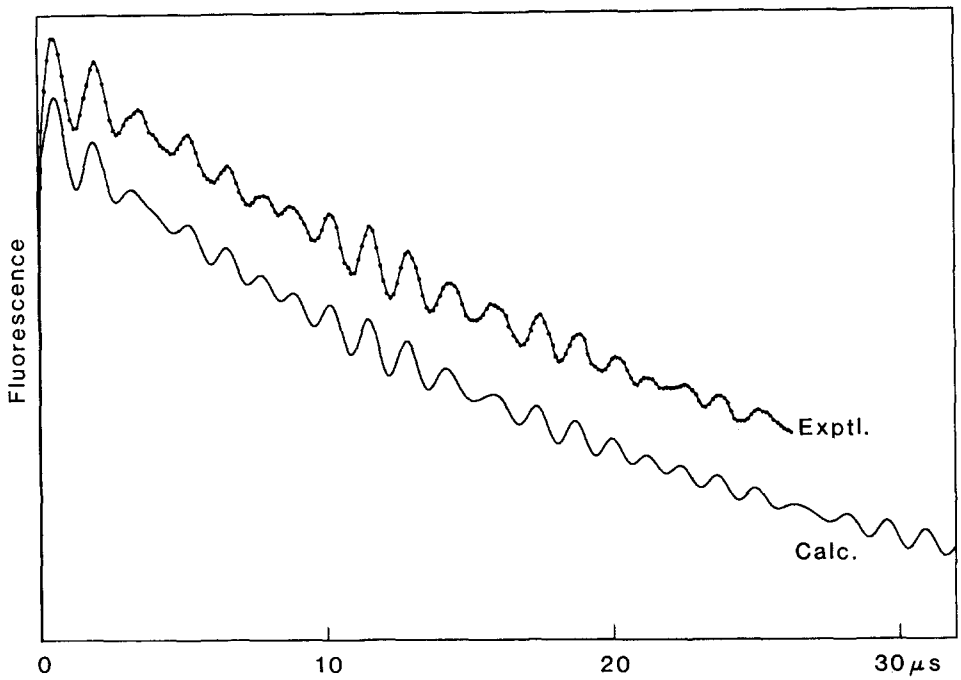

FIG. 4. Time resolved fluorescence decay observed after pulsed excitation of the F_2 $9_{09}-10_{0,10}$ transition at 16 840.90 cm^{-1}. The applied field is 2.6 G, detection polarization angle $\phi_D = 90°$, laser pulse duration 150 ns, and the total pressure is approximately 5×10^{-4} Torr. The calculated spectrum is displaced for clarity.

large spin splitting arises almost entirely from the upper vibronic level of this transition $[(\epsilon'_{bb}+\epsilon'_{cc})/2 = -0.0015,^{37}$ $(\epsilon'_{bb}+\epsilon'_{cc})/2 = -0.04^{34}]$. The R branch is congested and confused with P branch members of vibronic bands to the blue of this band. The line positions of the assigned P and R branch members of the $K'_a = 0$, 1, 2 stacks[38] show a highly perturbed excited state structure with approximate rotational constants $A' = 7.85$, $B' = 0.45$, and $C' = 0.39$ cm^{-1}.[34]

Figure 4 shows the time resolved fluorescence decay observed after pulsed excitation of a strong, well-isolated P branch member at moderate NO_2 pressure (5×10^{-4} Torr). The applied magnetic field causes the observed fluorescence to be modulated at three frequencies corresponding to the precessional motion of the hyperfine levels in the excited state ($I = 1$ for $^{14}N^{16}O_2$). Also in Fig. 4 is shown an empirical model of the decay where three modulation components of an exponential decay have been adjusted to best fit the observed decay. Data for the observed spectrum were accumulated for a period of 2 h.

Figure 5 presents a semilog plot of normalized fluorescence intensity vs time after excitation of the $F_1 3_{03}$ rotational level via its R branch transition at 16 851.98 cm^{-1}. The solid line represents the least squares fit to the data points and demonstrates an ex-

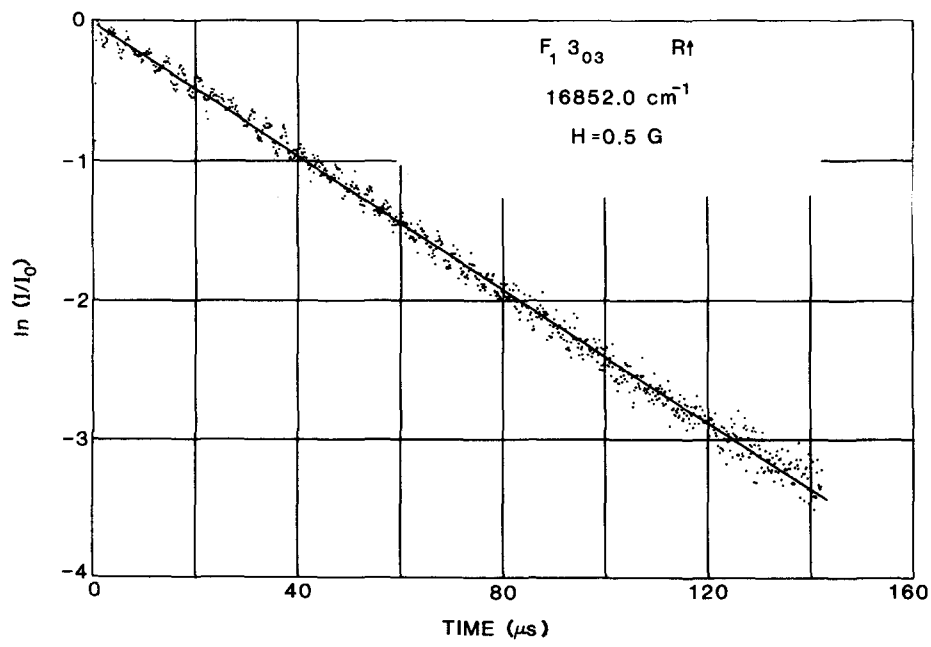

FIG. 5. Plot of $\ln(I/I_0)$ vs time of the emission observed following pulsed excitation of the F_1 $3_{03}-2_{02}$ transition at 16 851.98 cm^{-1}. The applied field is 0.5 G, detection polarization angle $\phi_D = 0°$, laser pulse duration 150 ns, and the total pressure is approximately 2×10^{-5} Torr. The solid line represents the linear least squares fit to the data points with a lifetime of 41 ± 2 μs.

ponential fluorescence relaxation "envelope" with a lifetime of a 41 ± 2 μs over a period of $3\frac{1}{2}$ lifetimes. The modulation induced by a 0.5 G field is clearly evident in the early time portion of this plot.

Figure 6(a) shows the real part of the Fourier transform of the decay under the same conditions as in Fig. 5. For brevity, we refer to the real part of the Fourier transform of the decay signal as the ZQB spectrum. The ZQB spectrum must be symmetrical about zero frequency for any real decay signal. A small portion of the negative (and redundant) spectrum is shown to compare the feature at zero frequency with those at nonzero frequency.

If we assume that all three hyperfine components of a fine structure level have the same decay rates Γ_0 and Γ_2, then from Sec. II we would predict the form of the decay from such a fine structure level to be

$$I(t) = \sum_{\kappa=-1}^{1} a_\kappa e^{-\Gamma_0 t} + \frac{b_\kappa}{2}\left[1 + 3\cos(2[\omega_\kappa t + \phi_D])\right] e^{-\Gamma_2 t}\,, \tag{19}$$

where the index ($\kappa = F_e - J_e$) determines a hyperfine level, the coefficients a_κ and b_κ are found from the appropriate sum of Eq. (16), and ω_κ are the hyperfine level Larmor frequencies. The Fourier transform of Eq. (19) is

$$F(\omega) = \bar{a}\,\frac{(\Gamma_0 - i\omega)}{\omega^2 + \Gamma_0^2} + \left(\frac{\bar{b}}{2}\right)\frac{(\Gamma_2 - i\omega)}{\omega^2 + \Gamma_2^2} + \frac{1}{4}\sum_{\kappa=-1}^{1} b_\kappa e^{\pm i 2\phi_D}\,\frac{[\Gamma_2 - i(\omega \pm 2\omega_\kappa)]}{(\omega \pm 2\omega_\kappa)^2 + \Gamma_2^2}\,, \tag{20}$$

where $\bar{a}$ and $\bar{b}$ are the mean of the a_κ and b_κ, respectively.

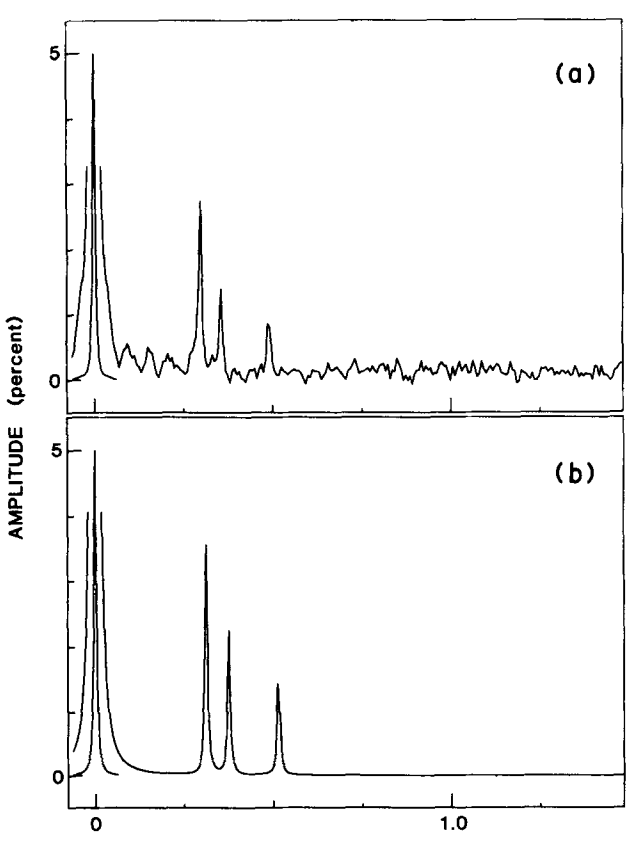

FIG. 6. The real part of the Fourier transform of the decay signal (ZQB spectrum). The horizontal scale is frequency ($\omega/2\pi$) and the vertical scale is the amplitude relative to the integrated fluorescence: (a) The observed ZQB spectrum after R branch excitation of the $F_1\,3_{03}$ level as in Fig. 5; and (b) The calculated ZQB spectrum for this level under the experimental conditions using Eq. (20). The zero frequency peaks in (a) and (b) are shown as insets reduced by a factor of 20.

TABLE I. Linewidths of the $F_1\,3_{03}$ level [see Fig. 6(a)].

Peak position (kHz)	0	300	356	491
g Factor	•••	0.21 ± 0.01	0.25 ± 0.01	0.35 ± 0.02
Linewidth FWHM (kHz)	7.7[a]	11	11	14
Inhomogeneous broadening (kHz)[b]	•••	2.9	3.5	4.9

[a]Obtained from a linear least squares fit of $\ln(I)$ vs t.
[b]Calculated from the g factors given in the first row and a magnetic field spatial inhomogeneity over the detection region of 5 mG.

The results on the $F_1\,3_{03}$ level of this band may now be conveniently discussed in terms of its experimentally observed ZQB spectrum and Eq. (20). The zero frequency peak in Fig. 6(a) corresponds to the Fourier transform of the decay envelope (shown to be exponential from Fig. 5). We see from Eq. (20) that in general this zero frequency feature is the sum of two Lorentzian line shapes with HWHM of Γ_0 and Γ_2. However, evaluation of $\bar{a}$ and $\bar{b}$ show that this feature is usually dominated by the first term in Eq. (20), e.g., $\bar{a}/\bar{b} = 10$ for large F_e and $|F_e - F_i| = |F_e - F_f| = 1$. Therefore, to good approximation the linewidth of this feature can be used to determine Γ_0. This approximation becomes exact for a choice of $\phi_D = 54.74°$ at zero field.

The three features near 400 kHz in Fig. 6 correspond to the third term in Eq. (20). Ideally, their linewidth directly determines the value for Γ_2. In this experiment however, these features are subject to broadening due to the spatial inhomogeneity of the applied magnetic field over the sample dimensions. The effect of this inhomogeneous broadening can be evaluated using the linear Zeeman Hamiltonian of Eq. (12) and the measured spatial variation of the magnetic field.

The observed linewidths of the ZQB spectrum shown in Fig. 6(a) are summarized in Table I. From column 1 it is seen that Γ_0 is approximately 7.7 KHz (FWHM). The remainder of the columns show that the linewidths associated with the quantum beats from the three hyperfine components are much larger, but when broadening by the magnetic field inhomogeneity is taken into consideration (last row), then it is concluded that $\Gamma_0 = \Gamma_2$ in each case. This conclusion is valid for the experimental conditions under which Fig. 5 was re-

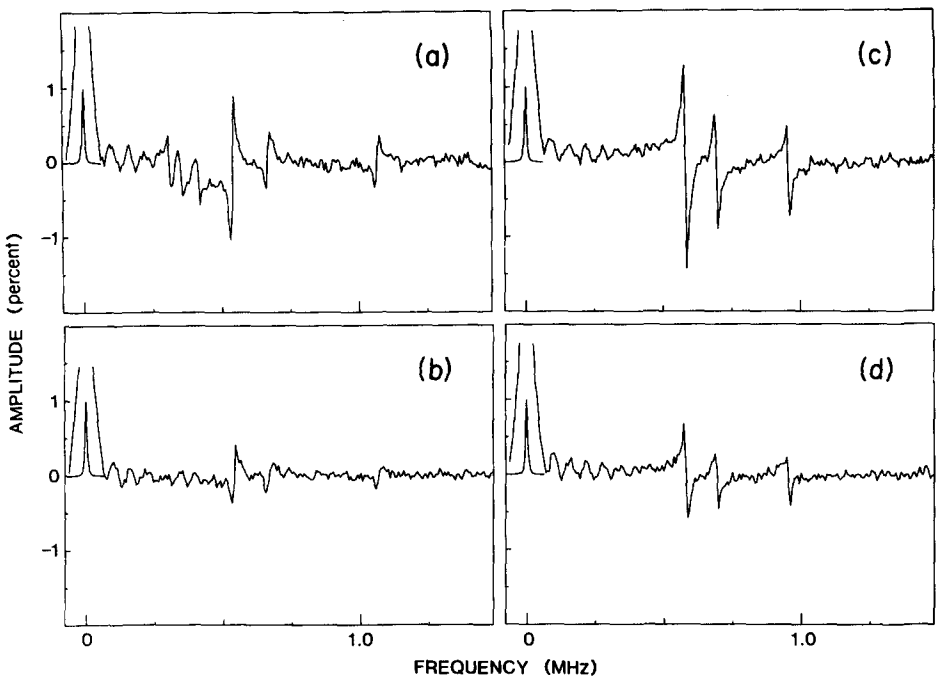

FIG. 7. ZQB spectra of the two fine structure components of the 3_{03} rotational level observed at 1.0 G and $\phi_D = +45°$; (a) R branch excitation of $F_2 3_{03}$; (b) P branch excitation of $F_2 3_{03}$; (c) R branch excitation of $F_1 3_{03}$; (d) P branch excitation of $F_1 3_{03}$. The zero frequency peaks are shown as insets reduced by a factor of 100.

corded, namely, total pressure of about 2×10^{-5} Torr. The same behavior is found for all other levels studied. Hence we conclude that *at total pressures* $\leq 2\times10^{-5}$ *Torr there is no process, collisional or intrinsic, that causes the spatial coherence of the* NO_2 *excited state to decay faster than the excited state population.*

Figure 6(b) shows a simulation of the ZQB spectrum in Fig. 6(a) where the coefficients in Eq. (20) have been evaluated using Eqs. (16), (17), and (18). In the simulation we have assumed $\Gamma_0 = \Gamma_2 = 7.7$ kHz. Furthermore, the coefficients a_κ and b_κ have been determined in a sum over F_i, F_f weighted by simple symmetric top line strengths.[39] Comparison of the observed and calculated ZQB spectra show an apparent reduction in the observed modulation amplitude $(b_\kappa/\bar{a})$. Several experimental nonidealities, such as finite excitation/detection polarization extinction ratios, finite detection solid angle effects, and imperfect selection of a single fine structure transition in excitation, could explain this discrepancy. Perhaps less evident is a slight reduction in the observed beat frequencies relative to those predicted from Eq. (18). This shift is well outside experimental error and must be considered significant.

Figure 7 shows the ZQB spectra observed from the two spin components of the 3_{03} rotational level each excited via both its R and P branch transitions. These transitions are indicated by the features marked "a" and "b" in the excitation spectrum in Fig. 3. As predicted from Eq. (16) the observed beat frequencies in the ZQB spectrum are solely determined from the excited state but the modulation amplitude depends on details of the absorption and emission steps. Reduced modulation amplitude for P branch relative to R branch excitation is strongly evident only in low J_e states. The choice of the detection polarization angle $\phi_D = +45°$ in these spectra allow the direct determination of the sign of the excited state g factors and therefore unambiguous spin assignment of the excited state from the observed phase of the dispersion line shape. Because several pump transitions lie within the Doppler limited excitation bandwidth, additional quantum beats are observed. They appear as periodic structure to the low frequency side of the beats arising from the 3_{03} level in all the spectra in Fig. 7 [see Fig. 7(a) in particular]. In all cases these beats are magnetic field-induced and disappear at zero field.

Figure 8 presents a plot of observed beat frequencies as a function of field strength for the F_1 3_{03} and F_1 3_{12} rotational levels of this band. Linear least squares analysis of this data shows that, to within experimental error, the Zeeman energy of the excited state is proportional to the applied field. Furthermore, the zero frequency intercept of the six hyperfine levels represented in the plot has a standard deviation of 1.6 mG and coincides precisely with zero magnetic field determined by level crossing. From this we conclude that the linear form of the Zeeman Hamiltonian [Eq. (12)] is valid and *no decoupling of the intrinsic angular momentum structure of the excited state is caused by fields up to* 2 *G*. However, the observed g factors of these levels differ markedly from those predicted from Eq. (18).

Table II summarizes the g factor information for some excited levels in this band. Table III lists the excitation transition frequencies used in the study of these levels. As indicated in Sec. II, the pattern of g factors of the hyperfine components comprising a single fine structure level may be interpreted in terms of the angular momentum coupling giving rise to a magnetic moment in a state of well defined total angular momentum J in the absence of hyperfine structure. The coupling of nuclear spin to this state determines the g factor of the levels of total angular momentum F. Pursuing this, we recognize

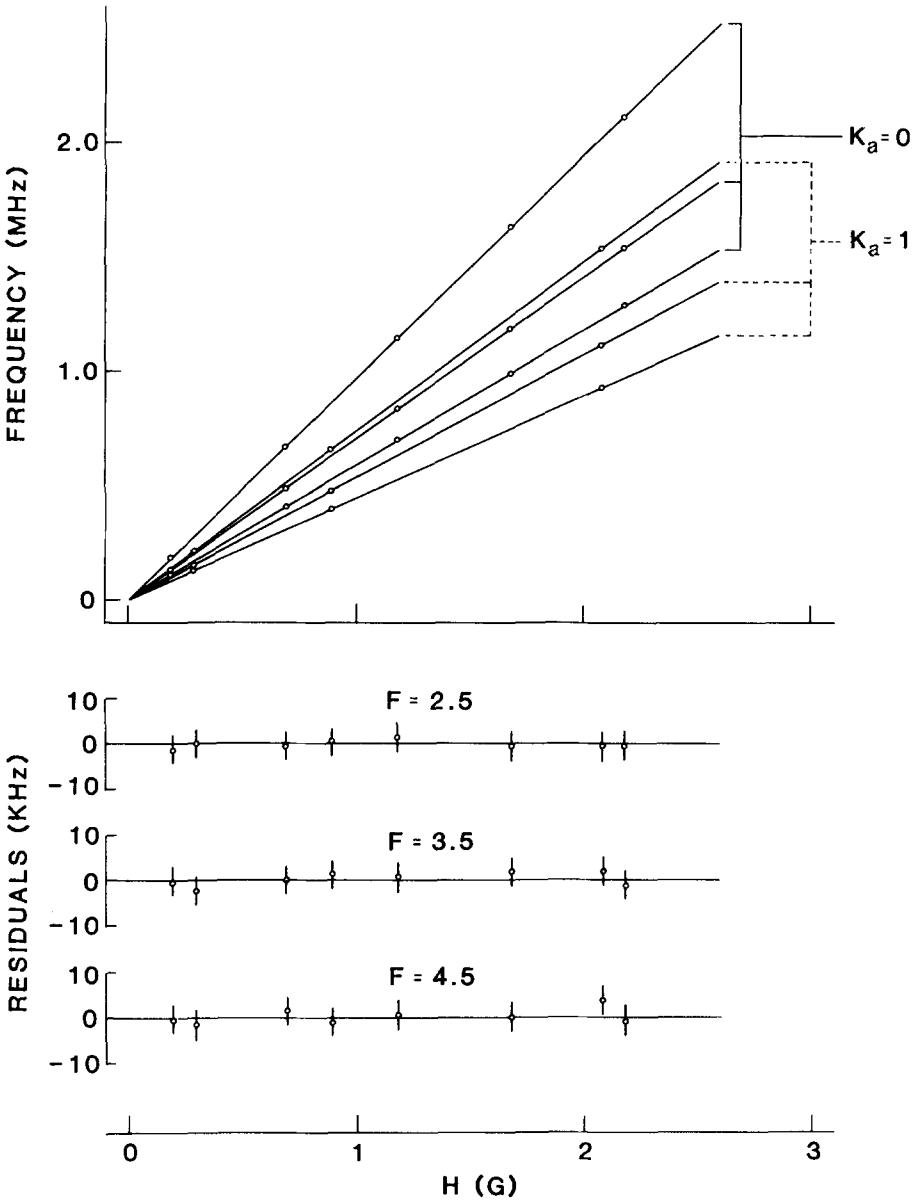

FIG. 8. Plot of observed ZQB frequencies vs applied magnetic field strength for the $F_1\,3_{03}$ (denoted $K_a = 0$) and $F_1\,3_{12}$ (denoted $K_a = 1$) excited levels. The residuals of a linear least squares fit to the data points are shown below grouped by the excited state total angular momentum F. The error bars shown are ±3 kHz.

TABLE II. Excited state g factors. (Calculated values are shown in parentheses.)

Excited level	τ_0 (μs)	g_{-1}/g_J	g_0/g_J	g_{+1}/g_J	g_J	σ (%)
$F_1\,3_{03}$	45	0.781 (0.7778)[a]	0.935 (0.9365)	1.285 (1.2857)	0.271 (0.286 0)[b]	5.2±1.4
$F_2\,3_{03}$	49	0.714 (0.7143)	0.880 (0.8857)	1.407 (1.4000)	−0.277 (−0.286 0)	3.1±1.5
$F_1\,3_{13}$	53	0.779 (0.7778)	0.935 (0.9365)	1.286 (1.2857)	0.206 (0.286 0)	28.0±1.1
$F_1\,11_{0,11}$	68	0.92 (0.9200)	0.99 (0.9930)	1.09 (1.0870)	0.036 1 (0.087 06)	58.5±0.6
$F_2\,11_{0,11}$	55	0.914 (0.9130)	0.991 (0.9917)	1.096 (1.0952)	−0.079 2 (−0.087 06)	9.0±1.4
$F_1\,11_{1,10}$	62	0.91 (0.9200)	0.99 (0.9930)	1.10 (1.0870)	0.020 4 (0.087 06)	76.6±0.4
$F_2\,11_{1,10}$	55	0.914 (0.9130)	0.993 (0.9917)	1.093 (1.0952)	−0.071 8 (−0.087 06)	17.5±1.2

[a]The g_κ/g_J values are calculated from Eq. (17) where $\kappa \equiv (F_a - J_a)$.

[b]The g_J values are calculated from Eq. (18).

TABLE III. Excitation frequencies of levels reported in Table II.

Excited level	R branch transition (cm^{-1})	P branch transition (cm^{-1})
$F_1\ 3_{03}$	16 851.98	16 846.07
$F_2\ 3_{03}$	52.14	46.23
$F_1\ 3_{12}$	51.88	45.90
$F_1\ 11_{0,11}$	a	38.23
$F_2\ 11_{0,11}$	a	38.83
$F_1\ 11_{1,10}$	a	40.80
$F_2\ 11_{1,10}$	a	40.62

[a]Accurate line position not available due to spectral congestion.

$$g_J = \frac{1}{3}\sum_{\kappa=-1}^{1} g_\kappa\ , \tag{21}$$

where again $\kappa = (F_e - J_e)$ designates a hyperfine level and the g_κ are the observed g factors. In all cases to date the measured values of (g_κ/g_J) are predicted within experimental error by the limiting angular momentum coupling scheme $\mathbf{F} = \mathbf{J} + \mathbf{I}$ and Eq. (17). However, *the observed values of g_J differ significantly from those predicted by Hund's case b coupling and Eq.* (18). In analogy to diamagnetic shielding and the chemical shift we introduce the quantity

$$\sigma = \frac{\hat{g}_J - g_J}{\hat{g}_J}\ , \tag{22}$$

where g_J and $\hat{g}_J$ are the observed and the Hund's case b [Eq. (18)] g factors, respectively. *For all levels studied the value of σ is observed to be positive.* The uncertainty associated with σ shown in Table II arises primarily from error in the magnetic field calibration to which the measurement of g_K/g_J is immune.

Also shown in Table II are our best estimates of the zero pressure radiative lifetime τ_0 for different rotational levels in the 5933 Å band. The values of τ_0 should be treated as approximate due to the systematic effects of the effusion of emitting molecules from the detection region and the contamination of the emission with fluorescence from other excited states populated through blended absorption transitions. Both of these effects will lead to the observation of nonexponential total emission decay which may or may not be discernible at finite signal to noise. The pressure dependence of the total emission below 1×10^{-4} Torr indicates that our τ_0 estimates are not biased by collisional electronic quenching or vibrational relaxation. It should be noted that emitter effusion affects the observed population and alignment decay *equally* making only the absolute measure of τ_0 uncertain. Taking into account the possible error in the absolute measure of τ_0, the mild dependence of τ_0 on rotational level must still be regarded as significant.

V. DISCUSSION

The technique of quantum beat spectroscopy provides natural-linewidth-limited resolution of the level structure of excited states. As has been demonstrated here for NO_2, this technique gives independent values for the excited state radiative and alignment (coherence) decay rates. By observation of the response of the molecule to applied field, one obtains g values in the case of a magnetic field or polarizabilities (dipole moments) in the case of an electric field. Because all these measurements can be carried out in the same experiment, quantum beat spectroscopy can be advantageous compared to level crossing, optical radio frequency double resonance, or other coherence methods that lack time resolution.

The physical interpretation of excited electronic states is considerably more complicated for polyatomic molecules than for atoms or diatoms. The extension of simple pictures to the description of the isolated polyatomic state may suffer from loss of predictive power and insight when perturbations are so numerous as to be the rule rather than the exception. For sufficiently complex cases, statistical treatment of the state properties may quantitatively predict *average* values of observables. However, this statistical description may be dissatisfying when the detailed mechanical nature of the state can be obtained experimentally. The high resolution technique of quantum beats may provide this detailed information readily.

The ubiquity of zero-field quantum beat phenomena is evident in the literature. Zero-field quantum beats following pulsed optical excitation of rotationally cold molecules have been observed in the fluorescence of biacetyl,[40,41] methylglyoxal,[40] anthracene,[42] pyrazine,[43–45] pyrimidine,[44] and SO_2.[46] Zero-field quantum beats have also been observed at room temperature in the fluorescence of acetylene.[47] These experiments are similar to this study in that coherence prepared in the excited state is evident in the time dependence of the fluorescence which can be related to the excited state structure. However, the coherently prepared levels are nondegenerate due to the intrinsic energy level structure of the excited state, not due to the presence of an applied field. In this respect the phenomenon is similar to quantum beats arising from hyperfine structure in the excited state (as observed, for example, in Ca[48]). Zero-field quantum beats of the type recently observed[40–47] are difficult to interpret because the assignment of the contributing levels and even the form of the coupling between these levels is uncertain. Moreover, the coherence bandwidth of the optical excitation may provide an insufficient "window" from which to observe the complete excited state structure. Also, the angular properties of these zero-field quantum beats, important in the description of hyperfine and field-induced quantum beats, need to be investigated.

In the present study, we have *not* observed zero-field quantum beats in the NO_2 $\tilde{A}\ ^2B_2$ fluorescence. Hence, we conclude that the likelihood is rare of finding at zero field two or more excited levels optically connected to the same lower level within the excitation coherence bandwidth ($1/\pi T \approx 2$ MHz). However, with larger excitation coherence bandwidth ($1/\pi T > 100$ MHz) hyperfine quantum beats should be evident at zero field.

Detailed study of the magnetic field-induced quantum

beats provides clarification of some controversies in the NO_2 $\tilde{A}\ ^2B_2$ state properties. First, we find that the isolated excited state population and alignment decay exponentially with *equal* rates, at least for the levels investigated. There is no evidence for intrinsic dephasing and there is no need to invoke additional internal structure. Previously, Hanle effect measurements from this laboratory[20] on a room temperature sample (0.5 mTorr) of NO_2 suggested that alignment decayed more rapidly than population in the absence of collisions. To explain this anomaly, it was proposed that the NO_2 molecule had additional internal structure giving rise to intrinsic dephasing.[49] Since then, Bylicki and Weber[22] have repeated the Hanle effect measurements on a molecular beam of NO_2. The found that the population and alignment decayed at the same rate, indicating that the previous study was in error. Our results corroborate this finding. However, we do not know at this time what the source of error was in the work of Figger, Monts, and Zare.[20] Second, we find that although the hyperfine levels composing a single fine structure state have the same exponential decay rate, there is a mild dependence of this rate on $\mathbf{N}'$, $\mathbf{J}'$, and (K_a', K_c') within a vibronic band. This dependence is not smooth, however, and with the data presently available (about 30 rotational levels in this band) no clear pattern emerges. Third, the excited state demonstrates a linear Zeeman Hamiltonian for small magnetic fields (less than 2 G). No magnetic field uncoupling is found. This is in contradiction to the work of Bylicki, König, and Weber.[23] Fourth, the pattern of observed g factors arising from a single fine structure state is consistent with the coupling of angular momenta $\mathbf{F} = \mathbf{J} + \mathbf{I}$, but the mean value of this pattern g_J is not consistent with Hund's case b coupling in the $\tilde{A}$ state. The deviation from pure case b behavior, expressed by the parameter σ, varies irregularly with rotational state. Previous optical radio frequency double resonance measurements[22] only found this deviation for $K' \neq 0$ levels; we observe that $K' = 0$ levels fail to obey case b coupling as well.

We interpret the variation in τ_0 and σ as evidence for the existence of many weak and "local" electronic perturbations within the 5933 Å band. The variation of the radiative lifetime of cleanly resolved rotational levels in NO_2 has been observed before.[50] This lifetime behavior may be compared with the rotational dependence of the fluorescence quantum yield[51] and lifetime[52] in the $\tilde{A}$ state of formaldehyde. Although no collisionless photochemistry is available to the $\tilde{A}$ state of NO_2 at this energy, three other electronic states form a complicated "background" of possible interacting levels. The "character" of a particular $\tilde{A}$ state level may critically depend on the structure of these background (zeroth order noninteracting) levels nearby in energy. It is anticipated that the parameter σ may provide independent input into the electronic character of the rotationally resolved $\tilde{A}$ state and even into the nature and coupling of the background levels. At present, we have no satisfactory model to correlate the variation in lifetime, g factor, and term energy for the observed NO_2 $\tilde{A}$ state rotational levels, but an extension of these measurements to include more levels may provide a detailed understanding of these properties.

ACKNOWLEDGMENTS

This work is supported by the National Science Foundation under Grant NSF CHE 81-08823. R.N.Z. gratefully acknowledges support through the Shell Distinguished Chairs Program, funded by the Shell Companies Foundation, Inc.

[1] E. B. Alexandrov, At. Phys. 6, 521 (1979).
[2] S. Haroche, *High-Resolution Laser Spectroscopy*, edited by K. Shimoda (Springer, Berlin, 1976), Chap. 7.
[3] J.-C. Lehmann, Les Houches Session XXVII, *Frontiers in Laser Spectroscopy*, edited by R. Balian, S. Haroche, and S. Liberman (North–Holland, Amsterdam, 1977).
[4] J. N. Dodd and G. W. Series, *Progress in Atomic Spectroscopy*, edited by W. Hanle and H. Kleinpoppen (Plenum, New York, 1978), Part A Chap. 14.
[5] E. B. Alexandrov, Opt. Spectrosc. 17, 522 (1964).
[6] J. N. Dodd, D. M. Warington, and R. D. Kaul, Proc. Phys. Soc. 84, 176 (1964).
[7] W. Gornik, D. Kaiser, W. Lange, J. Luther, and H.-H. Schulz, Opt. Commun. 6, 327 (1972).
[8] A. Hese, A. Renn, and H. S. Schweda, Opt. Commun. 20, 385 (1977).
[9] R. Wallenstein, J. A. Paisner, and A. L. Schawlow, Phys. Rev. Lett. 32, 1333 (1974).
[10] M. Brieger, A. Hese, A. Renn, and A. Sodiek, Chem. Phys. Lett. 76, 465 (1980).
[11] G. Gouedard and J. C. Lehmann, J. Phys. Lett. 40, L119 (1979).
[12] P. Lebow, R. Raab, and H. Metcalf, Phys. Rev. Lett. 42, 85 (1979); F. Raab, T. Bergman, D. Lieberman, and H. Metcalf, Opt. Lett. 5, 427 (1980).
[13] M. Brieger, A. Hese, A. Renn, and A. Sodiek, Chem. Phys. Lett. 78, 153 (1981).
[14] H. S. Schweda, A. Renn, and A. Hese, *Thirty Fifth Symposium on Molecular Spectroscopy*, *MF*8, The Ohio State University, 1980.
[15] D. Hsu, D. L. Monts, and R. N. Zare, *The Spectral Atlas of Nitrogen Dioxide* (Academic, New York, 1978).
[16] C. F. Jackels and E. R. Davidson, J. Chem. Phys. 65, 2941 (1976).
[17] D. Neuberger and A. B. F. Duncan, J. Chem. Phys. 22, 1693 (1954).
[18] F. Paech, R. Schmiedl, and W. Demtröder, J. Chem. Phys. 63, 4369 (1975).
[19] M. Bixon and J. Jortner, J. Chem. Phys. 50, 4061 (1969).
[20] H. Figger, D. L. Monts, and R. N. Zare, J. Mol. Spectrosc. 68, 388 (1977).
[21] H. G. Weber, P. J. Brucat, W. Demtröder, and R. N. Zare, J. Mol. Spectrosc. 75, 58 (1979).
[22] F. Bylicki and H. G. Weber, Chem. Phys. Lett. 79, 517 (1981).
[23] F. Bylicki, F. König, and H. G. Weber, Chem. Phys. Lett. 88, 142 (1982).
[24] R. W. Wood, Philos. Mag. 16, 184 (1908).
[25] R. N. Zare, J. Chem. Phys. 45, 4510 (1966).
[26] U. Fano, Rev. Mod. Phys. 29, 74 (1957).
[27] M. Sargent III, M. O. Scully, and W. E. Lamb, Jr., *Laser Physics* (Addison–Wesley, Reading, Massachusetts, 1974).
[28] M. P. Silverman, S. Haroche, and M. Gross, Phys. Rev. A 18, 1507, 1517 (1978).
[29] K. Blum, *Density Matrix Theory and Applications* (Plenum, New York, 1981), Chap. 4.
[30] W. E. Baylis, *Progress in Atomic Spectroscopy*, edited by W. Hanle and H. Kleinpoppen (Plenum, New York, 1979), Part B, Chap. 28.
[31] J. A. Paisner, Ph.D. thesis, Stanford University, Stanford, 1974.
[32] S. Goudsmit and R. F. Bacher, Z. Phys. 66, 13 (1930).

[33]S. Gerstenkorn and P. Luc, *Atlas du Spectre d'Absorption de la Molecule d'Iode* 14 800–20 000 cm^{-1}, edition du Centre National de la Recherche Scientifique, Paris, 1978.
[34]C. G. Stevens and R. N. Zare, J. Mol. Spectrosc. **56**, 167 (1975).
[35]T. Tanaka, R. W. Field, and D. O. Harris, J. Mol. Spectrosc. **56**, 188 (1975).
[36]A number of measurements indicate that the $\tilde{X}$ (000) state is the lower level of the 5933 Å band. Perhaps the most compelling of these is ground state MODR observed in Ref. 35.
[37]G. R. Bird, J. C. Baird, A. W. Jacke, J. A. Hodgeson, R. F. Curl, Jr., A. C. Kimble, J. W. Bransford, J. Rastrup-Anderson, and J. Rosenthal, J. Chem. Phys. **40**, 3378 (1964).
[38]Transitions thought (Ref. 35) to belong to the $K_a' = 3$, 4 stacks of this band are probably from a vibronic band to the blue of the 5933 Å band. See D. L. Monts and R. N. Zare, J. Mol. Spectrosc. **65**, 167 (1977).
[39]The fine structure line strengths were taken from G. Herzberg, *Molecular Spectra and Molecular Structure* (D. Van Nostrand, Princeton, 1950), Vol. I. The hyperfine line strengths were taken from C. H. Townes and A. L. Schawlow, *Microwave Spectroscopy* (Dover, New York, 1975), p. 125.
[40]J. Chaiken, M. Gurnick, and J. D. McDonald, J. Chem. Phys. **74**, 106 (1981).
[41]W. Henke, H. L. Selzle, T. R. Hays, S. H. Lin, and E. W. Schlag, Chem. Phys. Lett. **77**, 448 (1981).
[42]W. R. Lambert, P. M. Felker, and A. H. Zewail, J. Chem. Phys. **75**, 5958 (1981).
[43]B. J. Van den Meer, H. Th. Jonkman, G. M. ter Horst, and J. Kommandeur, J. Chem. Phys. **76**, 2099 (1982).
[44]S. Okajima, H. Sargusa, and E. C. Lim, J. Chem. Phys. **76**, 2096 (1982).
[45]P. M. Felker, W. R. Lambert, and A. H. Zewail, Chem. Phys. Lett. **89**, 309 (1982).
[46]W. Sharfin, M. Ivanco, and S. C. Wallace, J. Chem. Phys. **76**, 2095 (1982).
[47]E. Abramson, C. Kittrell, J. L. Kinsey, and R. W. Field, J. Chem. Phys. **76**, 2293 (1982).
[48]S. Haroche, J. A. Paisner, and A. L. Schawlow, Phys. Rev. Lett. **30**, 948 (1973).
[49]H. G. Weber, P. J. Brucat, and R. N. Zare, Chem. Phys. Lett. **60**, 179 (1979).
[50]D. L. Monts, B. Soep, and R. N. Zare, J. Mol. Spectrosc. **77**, 402 (1979).
[51]K. Shibuya and E. K. C. Lee, J. Chem. Phys. **69**, 5558 (1978).
[52]J. C. Weisshar and C. B. Moore, J. Chem. Phys. **70**, 5135 (1979).